The Role of Shape in Determining Molecular Motions

Mingyang Lu* and Jianpeng Ma*†
*Department of Biochemistry and Molecular Biology, Baylor College of Medicine, Houston, Texas 77030; and †Department of Bioengineering, Rice University, Houston, Texas 77005

ABSTRACT We examined the role of molecular shape in determining the patterns of low-frequency deformational motions of biological macromolecules. The low-frequency subspace of eigenvectors in normal mode analysis was found to be robustly similar upon randomization of the Hessian matrix elements as long as the structure of the matrix is maintained, which indicates that the global shape of molecules plays a more dominant role in determining the highly anisotropic low-frequency motions than the absolute values of stiffness and directionality of local interactions. The results provided a quantitative foundation for the validity of elastic normal mode analysis.

INTRODUCTION

For more than two decades, normal mode analysis (NMA) has played an important role in modeling harmonic vibrations of protein structures (1–4), especially in modeling large-scale deformational motions of supramolecular complexes (5–14). In recent years, this classic method has been revitalized by a new paradigm—elastic normal mode analysis (eNMA) (15,16)—which in many applications seems to be as effective as, and in other applications even more powerful than, the conventional NMA (for a review, see Ma (17)). In eNMA, a protein structure is represented by a linear elastic network regardless of the detailed chemical structure and then the standard procedure of NMA is applied to a linear potential function of the network. As shown in numerous cases (18–34), despite drastic differences in the forms of potential function, the low-frequency eigenvectors calculated by eNMA closely resemble those calculated from more accurate molecular mechanics potential functions such as a CHARMM force field (35). Such an insensibility of low-frequency modes to a force field provided a foundation for successful applications of eNMA to coarse-grained representation of protein models. The coarse-grained representations can be based on either C_α atoms (16) or a subset of C_α atoms (36), or on-lattice construction of protein structures (37), or even an elastic network derived from low-resolution density maps delivered by electron cryomicroscopy (cryo-EM) (38,39), in which case the positions of nodes of the network placed in the continuous density maps are not correlated with the positions of any real atoms. In all these cases, the most meaningful information retained in the models used for eNMA is the shape of the molecules.

Despite the phenomenal success of eNMA, however, one lingering question is not satisfactorily answered: why does eNMA work so well with such drastically coarse-grained representations of biomolecules? The commonly accepted explanation is that for large and densely packed systems like proteins, the low-frequency deformational modes are not sensitive to the local structural connectivity, rather it depends on the overall shape of the molecules (17). Although this is an intriguing argument, it has not so far been quantitatively demonstrated. In fact, as a common practice, the similarity of eigenvectors from eNMA to the ones computed from realistic molecular mechanics force fields is often visually compared.

In this short article, we report some new results regarding this issue. We demonstrate that for any compact system that contains components with finite interaction distance, as long as the structure of the Hessian matrix (positions of nonzero and zero elements) is maintained, the low-frequency subspace of eigenvectors remains robustly similar even with completely randomized (nonzero) matrix elements. Since the elements of the Hessian matrix contain information on the strength and directionality of local molecular interactions, to randomize them is, as an approximation, to generalize the case into any kind of molecular interaction. Therefore, if the low-frequency subspace of eigenvector does not change upon matrix randomization, it is reasonable to argue that the following two commonly used schemes of harmonic modal analysis are just two special cases included in the randomized set—the scheme in NMA, in which the strength and directionality of interactions is derived from more accurate potential functions, and the scheme in eNMA with coarse-grained representations. Moreover, since the structure of the Hessian matrix is completely determined by molecular shape, therefore, if the above conclusion is true, it indicates that the low-frequency subspace of eigenvector is not sensitive to the detailed forms of molecular interactions, rather it is predominately determined by the shape of the molecule.

METHODS AND RESULTS

To demonstrate our point, let's start with two relatively simple cases. We first computed normal modes of an all-helical protein (myoglobin, Protein Data Bank code 1bvc, 153

Submitted May 5, 2005, and accepted for publication July 15, 2005.

Address reprint requests to Jianpeng Ma, 1 Baylor Plaza, BCM-125, Baylor College of Medicine, Houston, TX 77030. Tel.: 713-798-8187; Fax: 713-796-9438; E-mail: jpma@bcm.tmc.edu.

0006-3495/05/10/2395/07 $2.00

doi: 10.1529/biophysj.105.065904

residues) and an all-sheet protein (human basic fibroblast growth factor, Protein Data Bank code 1bff, 129 residues) using C_α-based eNMA (with a cutoff distance of 13 Å) (16). The structures of their respective Hessian matrices were then used as a template for randomization. All the elements in the off-diagonal blocks (each block has a size of 3 × 3 and represents a pair of interactions) were randomized. We let the random variables obey uniform distribution ranging from 0.7 to 1.3. Our study showed that the absolute values of the random variables are not important just as in eNMA (the force constant is usually set to 1.0). However, the spread of variables and their distributions matter a lot (see further discussion later).

The elements in the diagonal blocks were set as the negative sum of the corresponding elements in the off-diagonal blocks in a row. The symmetry of the entire Hessian matrix was kept. Fig. 1 *a* shows the comparison of the components of eigenvectors of mode 7, 10, and 30 for both proteins. It is

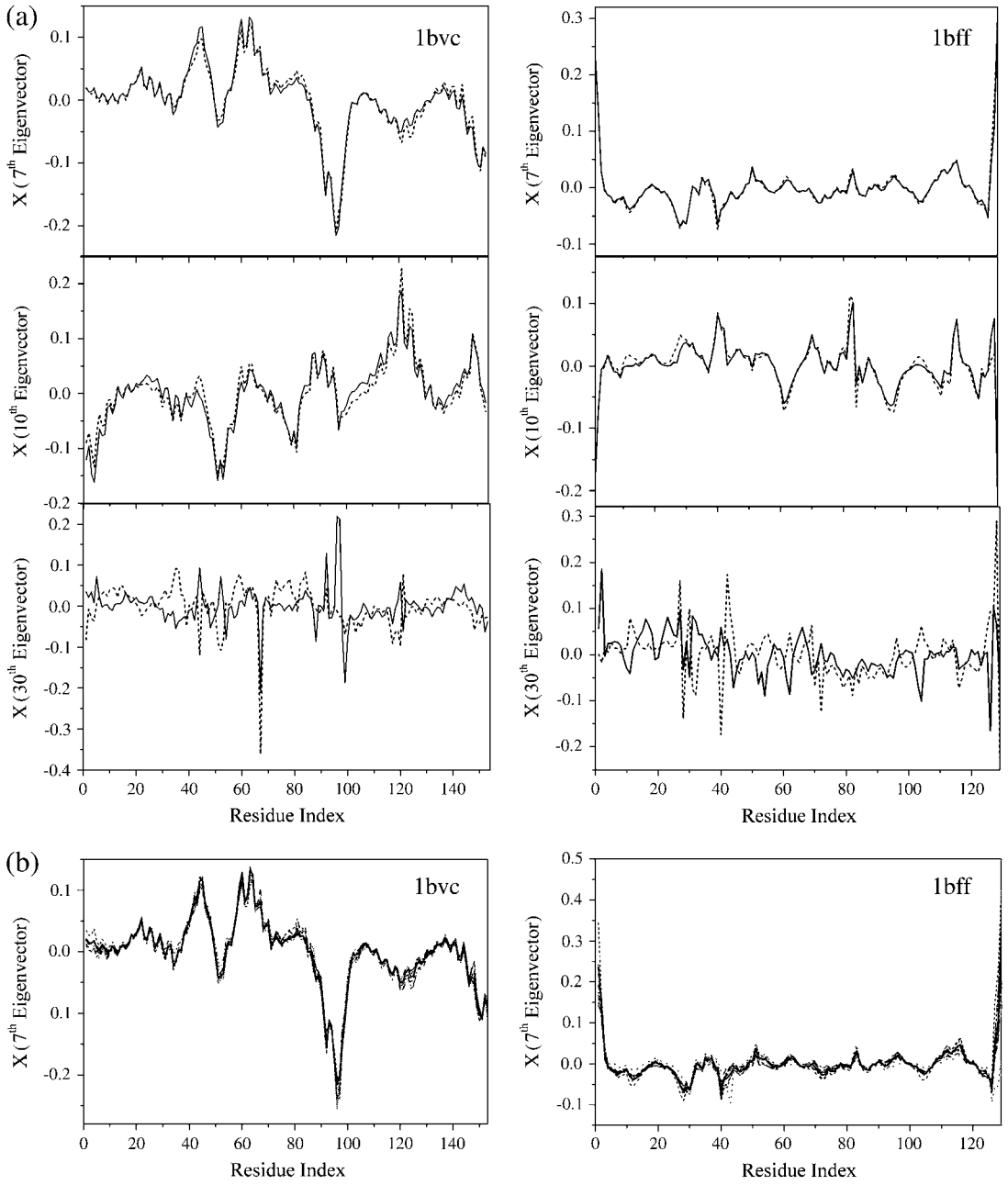

FIGURE 1 Comparison of eigenvector components. (*a*) For 7th, 10th, and 30th modes, only the *x* components are shown (other components show exactly the same tendency). The deviation between before (*solid line*) and after (*dotted line*) randomization increases with the frequency or modal index. (*b*) Eigenvectors for 7th modes upon 10 independent randomizations of matrix elements. For both *a* and *b*, results are shown for 1bvc (*left column*) and 1bff (*right column*).

clear that all components of the eigenvectors for mode 7 (the lowest-frequency mode) matched very well before and after the randomization. The level of matching decreases as the frequency goes up. In Fig. 1 *b*, we show the variation of mode 7 upon 10 independent randomizations of the Hessians. It is clear that this mode does not change much in both proteins. In Fig. 2, the dot products of modes before and after randomization were shown. If the dot product was calculated on a one-to-one basis along the modal index (*circles*), only a very few modes had high similarity (the values of dot product close to 1.0); the rest diversified quickly. If, however, a linear combination of modes was employed (*squares*), i.e., each eigenvector in the subspace after randomization was projected onto a linearly combined vector by the first 50 vibrational modes in the subspace before randomization, the subspace of low-frequency modes turned out to be very similar between two cases. These results indicate that the low-frequency subspace of eigenvectors is very robust upon randomization of matrix elements.

The above demonstration was based on the case in which the structure of the Hessian matrix was kept the same. Now we show the case in which the structure of the Hessian matrix was partially changed. As in Fig. 3, upon randomly swapping 5% ~ 10% positions of nonzero elements with those of zero elements, with a smaller incomplete low-frequency

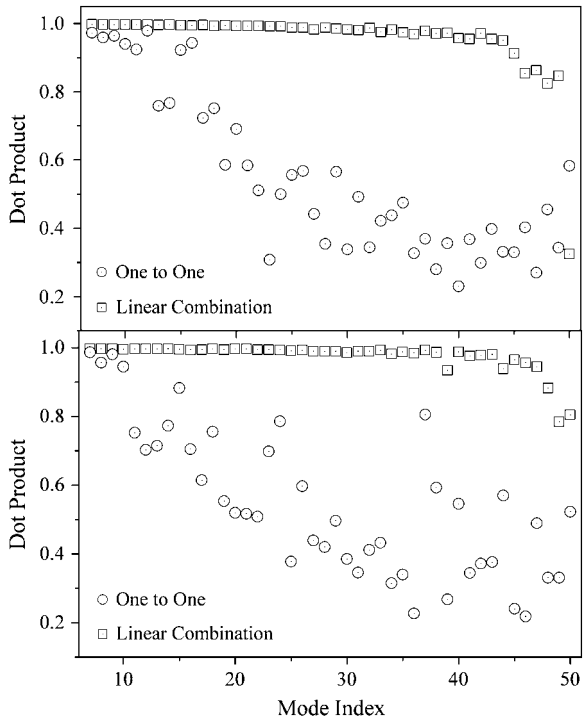

FIGURE 2 Quantitative comparison of eigenvectors for low-frequency subspace by dot products of vectors. The circles are for dot products of one-by-one based on the modal index. The squares are for dot products after a linear combination of the first 50 modes before randomization. The similarity is much better in low-frequency subspace by linear combination. Upper panel is for 1bvc and lower panel is for 1bff.

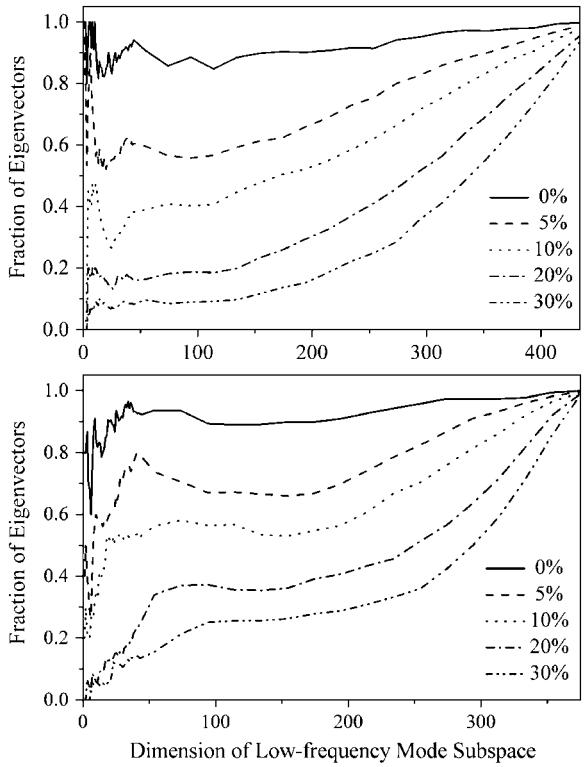

FIGURE 3 Effect of altering the structure of the Hessian matrix. As indicated in the main text, positions of a certain percent of nonzero elements were swapped with those of zero elements. As a consequence, the pattern of the low-frequency subspace of the eigenvector dramatically changes. For each curve, the *x* axis is the number of eigenvectors before the randomization used to form a linear combination basis set to express a single eigenvector after randomization. The *y* axis is the fraction of eigenvectors with the dot product value <0.9. Note the curves all converged to 1.0 at the large end of the basis set used for linear combinations, because one can always use a complete orthonormalized basis set to express any other vectors. What is the most interesting is when only incomplete low-frequency subsets of modes are used. Upper panel is for 1bvc and lower panel is for 1bff.

basis set, the eigenvectors after structure randomization can no longer be expressed by the subspace of low-frequency eigenvectors before the randomization, which sharply contrasts with the results in Fig. 2, where the low-frequency modes after randomization were expressed very well by linearly combined modes before randomization. Therefore, it suggests that the structure of the Hessian matrix is far more important in determining the nature of the low-frequency subspace of eigenvectors than the absolute values of matrix elements.

Having so far demonstrated the effect of randomization on the Hessian matrix in eMNA, we now show the case with the Hessian matrix computed by a realistic molecular mechanics force field, the CHARMM force field (35,40). We first computed the Hessian matrix based on a fully minimized myoglobin structure. Then, we adopted a special procedure to reduce, or to coarse-grain, the matrix from a size of $3N\times3N$ to $3n\times3n$ on the C_α-trace so as to be able to directly compare the results with C_α-based eNMA (N is the number

of atoms and n is the number of C_α atoms). To do so, we first summed up the elements of a block of elements in a mass-weighted CHARMM Hessian that belong to a particular pair of residues to reduce to a 3×3 block. The three principal component axes of this smaller block were then computed and projected back onto the vector connecting two C_α atoms to regenerate the values of elements for the smaller blocks. The projection obeys $\gamma^{\text{new}} \propto \sum_{k=1}^{3} \lambda_k (\vec{e}_k \cdot \vec{r}^{\,0})^2$, where λ_k, $\vec{e}_k$ ($k = 1,2,3$) are eigenvalues and eigenvectors of the 3×3 block and $\vec{r}^{\,0}$ is the direction vector between two C_α atoms. For simplicity, only the residue pairs with strong positive projections were kept; weak and negative ones were regarded as no interaction. The final resulting matrix was used as a coarse-grained Hessian for diagonalization. Fig. 4 *a* shows that the modes after the coarse-graining matched the original modes well in low-frequency subspace, indicating the validity of the coarse-graining procedure. Fig. 4 *b* shows the matching between coarse-grained CHARMM modes and eNMA modes, which once again shows the similarity of low-frequency modes between CHARMM and eNMA once they are reduced to the same level of coarse-graining. Here, the deviation of modes as the frequency goes up (Fig. 4 *b*) is somewhat quicker than that in Fig. 2. This is partly because the structure of the Hessian matrix reduced from CHARMM calculation is not exactly the same as that from eNMA since the two methods used different cutoff distances and magnitudes of interactions. Fig. 5 shows the detailed structure of the two matrices for myoglobin. The matrix of eNMA (using a residue-based cutoff of 13 Å) is larger, and its area of nonzero elements completely overlaps the area of the reduced CHARMM matrix (using an atom-based cutoff). What is really important, however, is that the two matrix structures are similar—one contains the other, thus the feature of low-frequency subspace is still similar. In fact, there have been numerous cases in which low-frequency modes from eNMA were used to approximate the modes traditionally computed by more accurate molecular mechanics force fields.

CONCLUDING DISCUSSION

In this study, we have quantitatively demonstrated that for a compact molecular structure such as that of a globular protein, the shape of the molecule plays a predominant role in determining the eigenvectors of low-frequency normal modes. It was shown that as long as the information of the overall molecular shape is maintained in the Hessian matrix, the low-frequency modes are all similar for a wide range of coarse-graining levels and for almost any potential function.

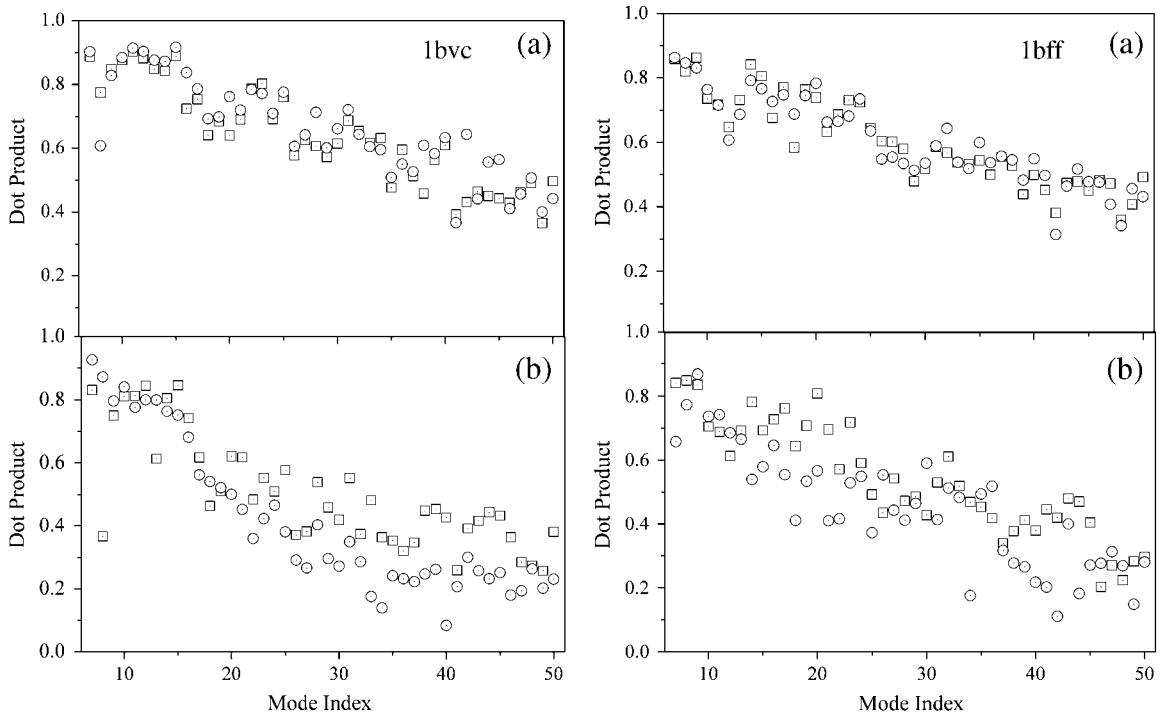

FIGURE 4 Comparison of eigenvectors for the low-frequency subspace for the coarse-grained Hessian matrix from CHARMM (results are shown for myoglobin 1bvc). The curves were computed in exactly the same way as in Fig.2. In upper panel (*a*), the squares are for comparison between eNMA calculation on the reduced CHARMM matrix and the C_α subspace of all-atom CHARMM eigenvectors (using eNMA low-frequency orthogonal subspace as a basis set). The circles are for comparison between an eNMA calculation on the matrix with the same structure as a reduced CHARMM matrix but all the force constants were set to one and the C_α subspace of all-atom CHARMM eigenvectors (using eNMA low-frequency subspace as a basis set). In the lower panel (*b*), the squares are for comparison between direct eNMA calculation on C_α atoms and the C_α subspace of all-atom CHARMM eigenvectors (using eNMA low-frequency subspace as a basis set). The circles are for comparison between eNMA calculation on a reduced CHARMM matrix and direct eNMA calculation on C_α atoms (using a low-frequency subspace of eNMA from reduced CHARMM as a basis set). Left column is for 1bvc and right column is for 1bff.

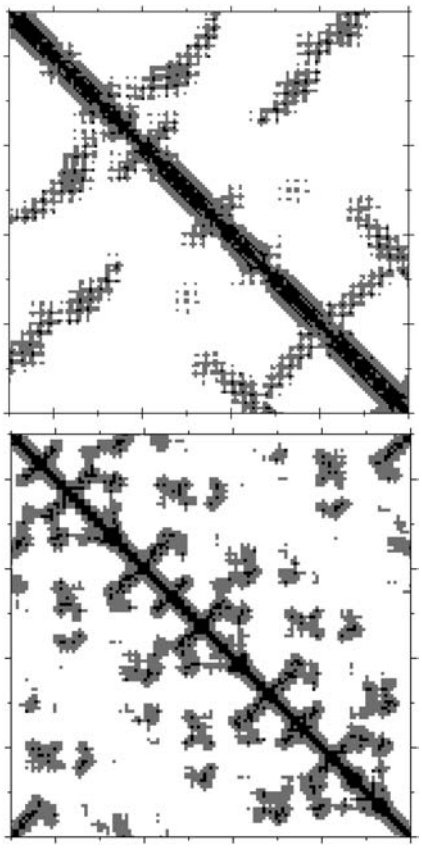

FIGURE 5 Hessian matrices. White area is for zero elements. Shaded is for eNMA based on C_α atoms. Solid is for the nonzero elements in Hessian reduced from the CHARMM matrix. The matrix of eNMA has more nonzero elements, but the two matrices have similar structure. One contains the other. Upper panel is for 1bvc and lower panel is for 1bff.

This conclusion was drawn from the study of the subset of low-frequency eigenvectors for Hessian matrices with randomized matrix elements, but with an identical matrix structure (the positions of nonzero and zero elements). The results further strengthen the foundation of the highly successful eNMA.

Moreover, in this work, although results were presented for only two small proteins, an all-helical protein (myoglobin) and an all-sheet protein (A-spectrin SH3 domain), the conclusion holds true for all compact globular proteins or protein domains, just as the fact that eNMA is universally successful for all those proteins.

Another important observation is that in randomizing Hessian matrix elements, it is better to use more uniform distributions of random numbers with a smaller spread. We believe that this is consistent with the fact that protein structures are relatively uniform in terms of the distribution of mass and strength of interactions at residue level (41). Imagine, for a bilobate molecule with drastically different stiffness in two domains, one would not be able to see the behavior we have seen. Such a conclusion is also in accord with the observation that eNMA with a uniform force constant is less effective in modeling the interfacial motions between protein and nucleic acid complexes precisely due to the difference in stiffness of the two types of molecules (42).

A point worth mentioning is that the low-frequency modes of any macromolecule are highly anisotropic. Therefore, one of the important implications of our results is that the anisotropic motions of molecules are determined by their shape. This is intuitively reasonable. If we take a two-domain protein such as lysozyme to compute low-frequency modes at any level of coarse-graining, it is guaranteed that we will get the classic hinge-bending mode because of the bilobate shape of the molecule (43–45). In fact, even if we reduce the representation of molecules to as simple as three points arranged in an angled fashion, we will still get the well-known bending mode as a triatomic water molecule. This example pictorially demonstrates that the global molecular shape determines its low-frequency anisotropic motions.

On the other hand, in the isotropic limit, the magnitudes of atomic fluctuation are mainly influenced by the local mass distribution. This was initially demonstrated in the pioneering work of the Gaussian network model (GNM) (46). Recently, it was also shown that a residue-based fluctuation profile could also be estimated by a simple relation of $1/n$, where n is the number of neighboring residues within a cutoff distance (47). The $1/n$ result is essentially a first-degree approximation of GNM, and the results of the two methods are almost identical with a larger cutoff distance (>10 Å). These isotropic methods are very effective in explaining the fact that the peaks of crystallographic B-factor profiles for globular proteins are almost always on the surface residues since, for a given cutoff distance, they are the ones with a smaller number of neighbors. Of course, an implicit assumption behind these isotropic calculations is that the globular proteins are uniform in packing density and interaction stiffness. This is why the isotropic calculations are more effective for compact globular proteins.

Finally, it is also reasonable to deduce from our results that a main task of evolution is to select the right shape of molecules so as to preserve certain types of motion for fulfilling the functions. This is particularly true for large supramolecular complexes in which motions of components are evolved to be optimally coupled to the motions of complexes just as in many manmade machines (for a review, see Ma (48)).

The authors thank the National Institutes of Health for support (R01-GM067801). M.L. was partially supported by a predoctoral fellowship from the W. M. Keck Foundation of the Gulf Coast Consortia through the Keck Center for Computational and Structural Biology.

REFERENCES

1. Brooks III, C. L., M. Karplus, and B. M. Pettitt. 1988. Proteins: a theoretical perspective of dynamics, structure, and thermodynamics. *Adv. Chem. Phys.* 71:1–249.
2. McCammon, J. A., and S. Harvey. 1987. Dynamics of Proteins and Nucleic Acids. Cambridge University Press, Cambridge.

3. Brooks, B. R., D. Janezic, and M. Karplus. 1995. Harmonic analysis of large systems. I. Methodology. *J. Comput. Chem.* 16:1522–1542.
4. Levitt, M., C. Sander, and P. S. Stern. 1985. Protein normal-mode dynamics: trypsin inhibitor, crambin, ribonuclease and lysozyme. *J. Mol. Biol.* 181:423–447.
5. Ma, J., and M. Karplus. 1998. The allosteric mechanism of the chaperonin GroEL: a dynamic analysis. *Proc. Natl. Acad. Sci. USA.* 95:8502–8507.
6. Ma, J., and M. Karplus. 1997. Ligand-induced conformational changes in *ras* p21: a normal mode and energy minimization analysis. *J. Mol. Biol.* 274:114–131.
7. Seno, Y., and N. Go. 1990. Deoxymyoglobin studied by the conformational normal mode analysis. I. Dynamics of globin and the heme-globin interaction. *J. Mol. Biol.* 216:95–109.
8. Seno, Y., and N. Go. 1990. Deoxymyoglobin studied by the conformational normal mode analysis II. The conformational change upon oxygenation. *J. Mol. Biol.* 216:111–126.
9. Thomas, A., M. J. Field, and D. Perahia. 1996. Analysis of the low-frequency normal modes of the R state of aspartate transcarbamylase and a comparison with the T state modes. *J. Mol. Biol.* 261:490–506.
10. Thomas, A., M. J. Field, L. Mouawad, and D. Perahia. 1996. Analysis of the low frequency normal modes of the T-state of aspartate transcarbamylase. *J. Mol. Biol.* 257:1070–1087.
11. Thomas, A., K. Hinsen, M. J. Field, and D. Perahia. 1999. Tertiary and quaternary conformational changes in aspartate transcarbamylase: a normal mode study. *Proteins.* 34:96–112.
12. Li, G., and Q. Cui. 2002. A coarse-grained normal mode approach for macromolecules: an efficient implementation and application to Ca(2+)-ATPase. *Biophys. J.* 83:2457–2474.
13. Cui, Q., G. Li, J. Ma, and M. Karplus. 2004. A normal mode analysis of structural plasticity in the biomolecular motor F(1)-ATPase. *J. Mol. Biol.* 340:345–372.
14. Krebs, W. G., V. Alexandrov, C. A. Wilson, N. Echols, H. Yu, and M. Gerstein. 2002. Normal mode analysis of macromolecular motions in a database framework: developing mode concentration as a useful classifying statistic. *Proteins.* 48:682–695.
15. Tirion, M. M. 1996. Large amplitude elastic motions in proteins from a single-parameter, atomic analysis. *Phys. Rev. Lett.* 77: 1905–1908.
16. Atilgan, A. R., S. R. Durell, R. L. Jernigan, M. C. Demirel, O. Keskin, and I. Bahar. 2001. Anisotropy of fluctuation dynamics of proteins with an elastic network model. *Biophys. J.* 80:505–515.
17. Ma, J. 2004. New advances in normal mode analysis of supermolecular complexes and applications to structural refinement. *Curr. Protein Pept. Sci.* 5:119–123.
18. Ming, D., Y. Kong, Y. Wu, and J. Ma. 2003. Simulation of F-actin filaments of several microns. *Biophys. J.* 85:27–35.
19. Ming, D., Y. Kong, S. J. Wakil, J. Brink, and J. Ma. 2002. Domain movements in human fatty acid synthase by quantized elastic deformational model. *Proc. Natl. Acad. Sci. USA.* 99: 7895–7899.
20. Kong, Y., D. Ming, Y. Wu, J. K. Stoops, Z. H. Zhou, and J. Ma. 2003. Conformational flexibility of pyruvate dehydrogenase complexes: a computational analysis by quantized elastic deformational model. *J. Mol. Biol.* 330:129–135.
21. Beuron, F., T. C. Flynn, J. Ma, H. Kondo, X. Zhang, and P. S. Freemont. 2003. Motions and negative cooperativity between p97 domains revealed by cryoelectron microscopy and quantized elastic deformational model. *J. Mol. Biol.* 327:619–629.
22. Keskin, O., I. Bahar, D. Flatow, D. G. Covell, and R. L. Jernigan. 2002. Molecular mechanisms of chaperonin GroEL-GroES function. *Biochemistry.* 41:491–501.
23. Wang, Y., A. J. Rader, I. Bahar, and R. L. Jernigan. 2004. Global ribosome motions revealed with elastic network model. *J. Struct. Biol.* 147:302–314.
24. Xu, C., D. Tobi, and I. Bahar. 2003. Allosteric changes in protein structure computed by a simple mechanical model: hemoglobin T↔R2 transition. *J. Mol. Biol.* 333:153–168.
25. Tama, F., M. Valle, J. Frank, and C. L. Brooks III. 2003. Dynamic reorganization of the functionally active ribosome explored by normal mode analysis and cryo-electron microscopy. *Proc. Natl. Acad. Sci. USA.* 100:9319–9323.
26. Tama, F., and C. L. Brooks III. 2002. The mechanism and pathway of pH induced swelling in cowpea chlorotic mottle virus. *J. Mol. Biol.* 318: 733–747.
27. Chacon, P., F. Tama, and W. Wriggers. 2003. Mega-dalton biomolecular motion captured from electron microscopy reconstructions. *J. Mol. Biol.* 326:485–492.
28. Miyashita, O., J. N. Onuchic, and P. G. Wolynes. 2003. Nonlinear elasticity, proteinquakes, and the energy landscapes of functional transitions in proteins. *Proc. Natl. Acad. Sci. USA.* 100: 12570–12575.
29. Kundu, S., J. S. Melton, D. C. Sorensen, and G. N. Phillips Jr. 2002. Dynamics of proteins in crystals: comparison of experiment with simple models. *Biophys. J.* 83:723–732.
30. Brink, J., S. J. Ludtke, Y. Kong, S. J. Wakil, J. Ma, and W. Chiu. 2004. Experimental verification of conformational variation of human fatty acid synthase as predicted by normal mode analysis. *Structure (Camb).* 12:185–191.
31. Carazo, J. M. 2004. Accessing information on the conformational flexibility of molecular machines. *Structure.* 12:170–171.
32. Tama, F., O. Miyashita, and C. L. Brooks III. 2004. Normal mode based flexible fitting of high-resolution structure into low-resolution experimental data from cryo-EM. *J. Struct. Biol.* 147: 315–326.
33. Wu, Y., and J. Ma. 2004. Normal-mode-based refinement of an F-actin model against fibre diffraction data. *Fibre Diff. Rev.* 12:25–28.
34. Wu, Y., and J. Ma. 2004. Refinement of F-actin model against fibre diffraction data by long-range normal modes. *Biophys. J.* 86: 116–124.
35. MacKerell Jr., A. D., D. Bashford Jr., M. Bellott, R. L. Dunbrack Jr., J. D. Evanseck, M. J. Field, S. Fischer, J. Gao, H. Guo, S. Ha, D. Joseph-McCarthy, L. Kuchnir, K. Kuczera, F. T. K. Lau, C. Mattos, S. Michnick, T. Ngo, D. T. Nguyen, B. Prodhom, W. E Reiher III, B. Roux, M. Schlenkrich, J. C. Smith, R. Stote, J. Straub, M. Watanabe, J. Wiorkiewicz-Kuczera, D. Yin, and M. Karplus. 1998. All-atom empirical potential for molecular modeling and dynamics studies of proteins. *J. Phys. Chem.* B102: 3586–3616.
36. Doruker, P., R. L. Jernigan, and I. Bahar. 2002. Dynamic of large proteins through hierarchical levels of coarse-grained structures. *J. Comput. Chem.* 23:119–127.
37. Doruker, P., and R. L. Jernigan. 2003. Functional motions can be extracted from on-lattice construction of protein structures. *Proteins.* 53:174–181.
38. Ming, D., Y. Kong, M. Lambert, Z. Huang, and J. Ma. 2002. How to describe protein motion without amino-acid sequence and atomic coordinates. *Proc. Natl. Acad. Sci. USA.* 99:8620–8625.
39. Tama, F., W. Wriggers, and C. L. Brooks. 2002. Exploring global distortions of biological macromolecules and assemblies from low-resolution structural information and elastic network theory. *J. Mol. Biol.* 321:297–305.
40. Brooks, B. R., R. E. Bruccoleri, B. D. Olafson, D. J. States, S. Swaminathan, and M. Karplus. 1983. CHARMM: a program for macromolecular energy, minimization, and dynamics calculations. *J. Comput. Chem.* 4:187–217.
41. Bagci, Z., A. Kloczkowski, R. L. Jernigan, and I. Bahar. 2003. The origin and extent of coarse-grained regularities in protein internal packing. *Proteins.* 53:56–67.
42. Van Wynsberghe, A. W., and Q. Cui. 2005. Comparison of mode analyses at different resolutions applied to nucleic acid systems. *Biophys. J.* In press.

43. Marques, O., and Y. H. Sanejouand. 1995. Hinge-bending motion in citrate synthase arising from normal mode calculations. *Proteins.* 23:557–560.

44. McCammon, J. A., B. R. Gelin, M. Karplus, and P. G. Wolynes. 1976. The hinge-bending mode in lysozyme. *Nature.* 262:325–326.

45. Brooks, B., and M. Karplus. 1985. Normal modes for specific motions of macromolecules: application to the hinge-bending mode of lysozyme. *Proc. Natl. Acad. Sci. USA.* 82:4995–4999.

46. Bahar, I., A. R. Atilgan, and B. Erman. 1997. Direct evaluation of thermal fluctuations in proteins using a single-parameter harmonic potential. *Fold. Des.* 2:173–181.

47. Halle, B. 2002. Flexibility and packing in proteins. *Proc. Natl. Acad. Sci. USA.* 99:1274–1279.

48. Ma, J. 2005. Usefulness and limitations of normal mode analysis in modeling dynamics of biomolecular complexes. *Structure.* 13: 373–380.